Cell Stem Cell
Resource

Induced Pluripotent Stem Cells from Patients with Huntington's Disease Show CAG-Repeat-Expansion-Associated Phenotypes

The HD iPSC Consortium[1,*]
[1]Membership of the consortium is provided in Document S2
*Correspondence: clive.svendsen@cshs.org
http://dx.doi.org/10.1016/j.stem.2012.04.027

SUMMARY

Huntington's disease (HD) is an inherited neurodegenerative disorder caused by an expanded stretch of CAG trinucleotide repeats that results in neuronal dysfunction and death. Here, The HD Consortium reports the generation and characterization of 14 induced pluripotent stem cell (iPSC) lines from HD patients and controls. Microarray profiling revealed CAG-repeat-expansion-associated gene expression patterns that distinguish patient lines from controls, and early onset versus late onset HD. Differentiated HD neural cells showed disease-associated changes in electrophysiology, metabolism, cell adhesion, and ultimately cell death for lines with both medium and longer CAG repeat expansions. The longer repeat lines were however the most vulnerable to cellular stressors and BDNF withdrawal, as assessed using a range of assays across consortium laboratories. The HD iPSC collection represents a unique and well-characterized resource to elucidate disease mechanisms in HD and provides a human stem cell platform for screening new candidate therapeutics.

INTRODUCTION

HD is an autosomal-dominant progressive neurodegenerative disease, characterized by movement, cognitive, and emotional disorders (Ross and Tabrizi, 2011; Walker, 2007). It is caused by an expanded CAG repeat in exon 1 of the Huntingtin (*HTT*) gene, which encodes an expanded polyglutamine stretch near the N terminus of the 350 kDa (HTT) protein (Consortium, 1993). The presence of more than 40 CAGs invariably causes disease within a normal lifespan, and longer repeats predict younger disease onset (Langbehn et al., 2010). Cell death occurs in many brain regions, but striatal medium spiny neurons (MSNs) expressing dopamine- and cAMP-regulated phosphoprotein (DARPP-32) undergo the greatest degeneration (Vonsattel et al., 2008). Although the mutation causing HD is known, our understanding of the pathogenesis is incomplete, and there is no treatment to delay the onset or slow the progression of HD.

Mutant HTT is widely expressed, and believed to induce neurodegeneration through abnormal interactions with other proteins. This leads to many cellular alterations, including abnormal vesicle recycling, loss of signaling by brain-derived neurotrophic factor (BDNF), excitotoxicity, perturbation of Ca^{2+} signaling, decreases in intracellular ATP levels, alterations of gene transcription, inhibition of protein clearance pathways, mitochondrial and metabolic disturbances, and ultimately cell death (Zuccato et al., 2010). Many of these observations were based on transfection of cDNAs encoding mutant HTT into primary nonhuman cells or rodent and human cell lines (reviewed in Ross and Tabrizi, 2011). In other studies, fibroblasts and lymphoblasts from HD patients show abnormal Ca^{2+} responses, enhanced toxicity in response to cellular stress, and CAG-repeat-expansion-associated altered ATP/ADP ratios (Seong et al., 2005). However, significant differences between rodent and human cells and between nonneuronal cells and neurons limit the utility of these models for accurately representing human disease. Ideally, in vitro mechanisms of neuronal death should be established in human neurons carrying the mutation.

Human embryonic stem cells (hESCs) can generate highly specified human cell populations, including DARPP-32-positive MSNs of the striatum (Aubry et al., 2008), and thus could provide a method for modeling HD. In fact, hESCs have been derived from embryos carrying HD mutations during preimplantation genetic diagnosis (Bradley et al., 2011). However, the limited access to HD embryos, the inability to assess the ultimate phenotype of the never-developed embryo, and the rare derivation of very long CAG expansions all restrict the utility of this approach. Many of these shortcomings could be overcome using cells from HD patients with known patterns of disease onset and duration that are reprogrammed to generate induced pluripotent stem cells (iPSCs; Takahashi et al., 2007; Yu et al., 2007). iPSCs, like hESCs, can be expanded indefinitely, and retain the potential to differentiate into neurons, and thus may hold great promise for modeling neurological diseases (for review see Mattis and Svendsen, 2011). Indeed, human iPSC lines have been generated from a variety of individuals, including HD patients (Park et al., 2008). However, just two studies have looked for phenotypic changes after differentiation using lines with lower repeat lengths and single assay techniques (Zhang et al., 2010; Camnasio et al., 2012).

Here, we report the generation of a panel of iPSC lines derived from a range of HD patient and control fibroblasts. Through an international consortium effort involving eight research groups, we show that these iPSC lines have clear, reproducible CAG-repeat-expansion-associated phenotypes upon differentiation. This report represents a unique stem cell resource for the

research and industrial community that may be used to both gain further mechanistic insights into HD and explore novel drug targets for this devastating disorder.

RESULTS

Neural Stem Cells Generated from HD iPSCs Express Mutant HTT and Show Specific Gene and Protein Expression Patterns

Fourteen HD and control iPSC lines were generated by the consortium (Tables S1 and S2 available online), eight of which were used in the various experiments within this paper (summarized in Table S3). The HD iPSC lines expressed the appropriate pluripotency markers (Figures 1A and S1A and S1B, available online) and normal karyotypes (Figures 1B and S1C). They also downregulated the exogenously expressed genes (except Klf4, which was turned off at later stages of differentiation; Figure S1A), and formed teratomas with all three lineages upon transplantation into immune-compromised mice (Figure S1D).

Neural stem cells (NSCs) were generated from the HD and control iPSC lines by lifting cells into a defined medium with epidermal growth factor (EGF) and fibroblast growth factor-2 (FGF-2), both at 100 ng/ml, as described previously (Ebert et al., 2009). These NSCs grew as spherical aggregates that were expandable for up to 50 passages and could be frozen or thawed with high efficiency, providing all consortium members with a reliable source of NSCs that could be differentiated into neurons and glia (via short protocol) and DARPP-32-expressing striatal neurons (via long protocol) (Figure 1C).

All NSC lines grew at similar rates and displayed genomic integrity by array comparative genomic hybridization (Agilent 244K arrays; data not shown). For most lines, the normal and expanded CAG repeat alleles exhibited only mild instability with passage or upon differentiation (data not shown). However, for one HD line (HD109i.1), we found complete stability of the short 19 CAG repeat and a minor increase (<10%) with passage of the long CAG repeat from 110 in the original fibroblast line to 118 after 26 passages of the NSCs (Figure 1D). Immunoblots of protein extracts with an antibody that recognizes normal and mutant HTT revealed that HD NSCs expressed both proteins, with the large CAG expansion in the HD180i.5 line showing slower migration on the gel (Figure 1E). Mutant HTT was also present in the HD60i.4 NSCs, but its similar size to normal HTT precluded its separation with the western blot parameters. An antibody that selectively detects expanded polyglutamine demonstrated the presence of mutated protein in the HD NSC lines (Figure 1F). Sections through growing NSC aggregates (Figure 1G) showed no expression of the pluripotentcy markers Oct4, SSEA4, or Tra-1-60 (data not shown) and robust expression of NSC markers nestin and PAX6 (Figure 1H).

Gene expression in three HD NSC lines (HD180i.5, HD109i.1, and HD60i.4) was compared to that in two control lines (HD33i.8 and HD21i.5) by whole-transcript expression profiling and analysis. Analysis of Variance (ANOVA) found 1,601 genes that were significantly differentially expressed with an absolute value of fold change >2. Hierarchical clustering showed a clear separation of HD and control NSC data sets (Figure 1I), with all HD data sets in one cluster and all controls in another. Of the 1,601 genes, key pathways were identified using Ingenuity Pathway Tools (IPA), including those involved in signaling, cell cycle, axonal guidance, and neuronal development (Table 1). Many of these changes are consistent with known transcriptional changes in HD, while others represent pathways not previously associated with HD pathogenesis. Some changes associated with specific categories were only present in lines with longer repeats, whereas others, such as changes in calcium signaling, showed effects specific to the 60 repeat range. Finally, there existed subtle differences between differentially expressed genes from highly expanded (HD180i.5 and HD109i.1) lines versus the HD60i.4 line, which would be expected based on our subsequent observations that there are differences in phenotypes between the lines (Table 1 and subsequent figures). Changes were validated by qPCR for 16 selected genes significantly altered in the HD NSCs (Table S5), supporting HD-related transcriptional deregulation even at this early stage of development. We also conducted protein profiling of the HD180i.5 NSCs relative to the control line using mass spectrometry and the iTRAQ method. IPA identified 356 upregulated and 191 downregulated proteins. Among the pathways enriched in upregulated proteins were those involving IGF-1 (Figure S2A; Zuccato et al., 2010). Gene expression and proteomics data were then compared by IPA, and several of the pathways modulated in the HD versus control lines were found to be in common. For example, a portion of the axonal guidance pathway involved in growth cone and extracellular matrix formation had altered protein expression, including BDNF and TRK receptors altered in HD (Figure S2B).

Neural Progenitor Cells Exhibit CAG Repeat-Associated Changes in Cytoskeleton, Adhesion, and Energetics

Previously a number of dominant changes in cell adhesion have been observed using immortalized and primary Hdh CAG knockin mouse striatal cells grown as monolayers on laminin (Reis et al., 2011). We first attempted to reproduce this phenotype by dissociating and acutely plating HD and control NSCs from spheres (short differentiation; Figure 1C) but found no difference in aggregation rates (data not shown). We then moved to identical neural progenitor cell (NPC) growth conditions as used in the mouse studies by plating HD and control NSCs onto laminin-coated coverslips with EGF and FGF-2 at 20 ng/ml (see Supplemental Experimental Procedures). Cells from all the HD lines grew well as an NPC monolayer under these conditions and were positive for nestin, Sox1, Sox2, Musashi, and Pax6 (Figure S3A) and were capable of differentiating into neurons and astrocytes upon mitogen removal (Figure S3B). However, HD NPCs had significantly less binding of phalloidin-peptide than control NPCs, suggesting changes in the actin cytoskeleton (Figure S3C). Furthermore, in a cell-cluster formation assay where cells are dissociated, plated, and allowed to form aggregates over time, all the HD NPCs showed significantly decreased cell-cell adhesion properties (Figures 2A and 2B). Previous studies using an allelic series of CAG knockin mouse ESC lines have shown dominant CAG length-dependent reductions in energy metabolism (Jacobsen et al., 2011). Here, all human-derived HD NPCs showed significantly decreased intracellular [ATP] (Figure 2C) and decreased [ATP/ADP] ratios (Figure 2D), suggesting that energy metabolism is compromised in both the HD60 and HD180 lines.

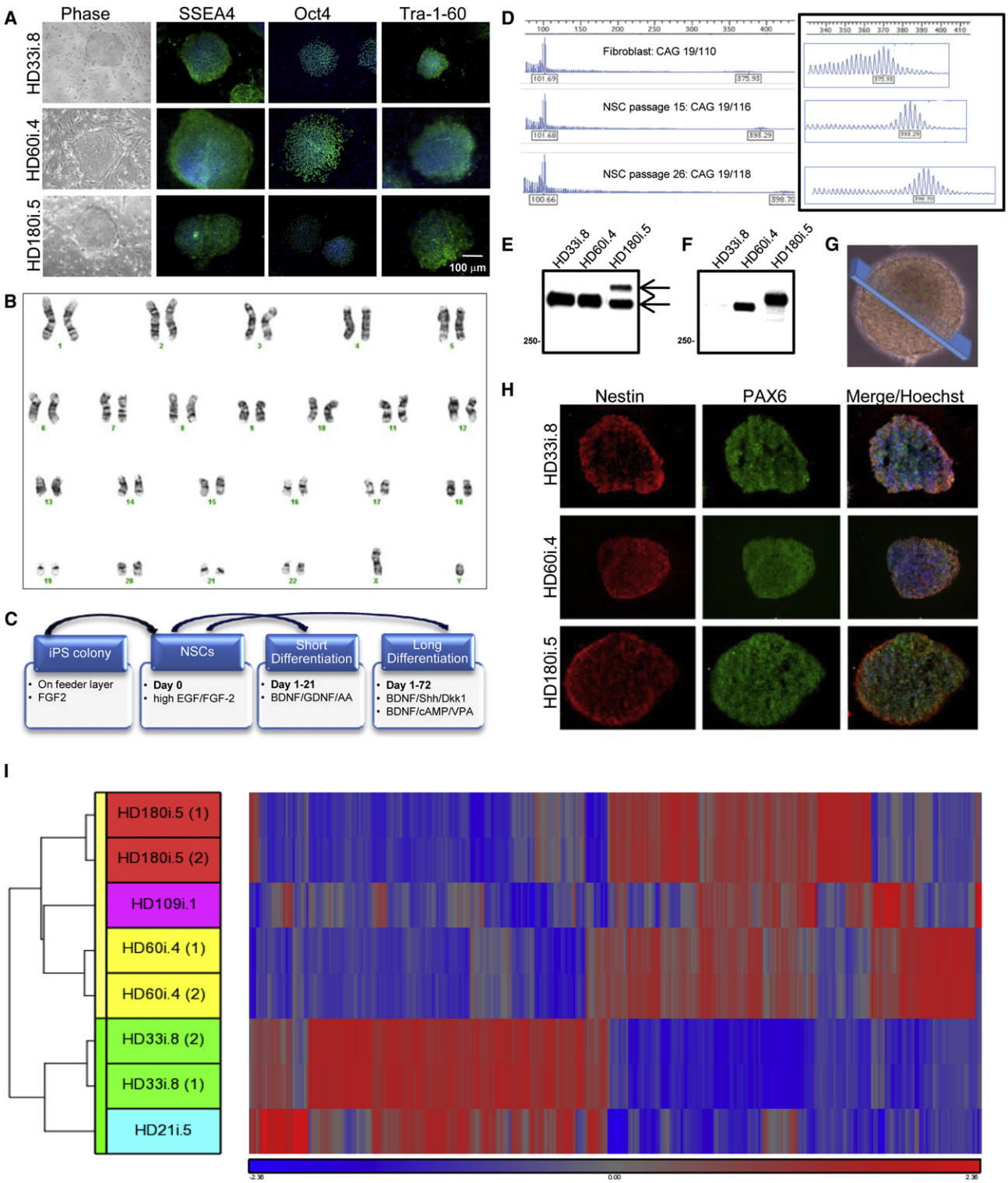

Figure 1. HD Fibroblasts are Reprogrammed into Karyotypically Normal iPSCs that Generate NSCs

(A) All reprogrammed lines form colonies (brightfield) and express the pluripotency markers Oct4, Tra-1-60, and SSEA4 by ICC.

(B) G-banding showed that the HD180i.5 line had a normal karyotype, which was representative of all lines at the colony and NSC stages.

(C) Schematic of the different differentiation protocols used.

(D) CAG repeat analysis in HD109i.1 fibroblasts and NSCs over 26 passages showed a small increase in repeat length over time.

(E) Western blots of HTT expression in iPSC-derived NSCs with the HTT antibody 2166 demonstrate normal (bottom arrow) and mutant (top arrow) HTT (epitope: amino acids 441–455).

Differentiated NSCs with Large CAG Expansion Show an Electrophysiology and Cell Death Phenotype

In order to establish whether HD NSCs could give rise to neurons with electrophysiological properties, NSCs were dissociated, plated on laminin, and allowed to differentiate up to 21 days in defined medium (short differentiation; Figure 1C) before having whole patch-clamp recordings performed upon them. MAP2a/b and GABA staining showed that all three lines generated neurons (Figure 3A) with functional expression of voltage-activated K^+ currents (Figure 3B), voltage-activated Na^+ currents (Figure 3C), voltage-activated Ca^{2+} currents (Figure 3D), and $GABA_A$ receptor Cl^- currents (Figure 3E). Maturing neurons from all lines also generated induced (Figure 3F) and spontaneous (Figure 3G) action potentials that correlated well with expression of voltage-gated Na^+ channels (Table S4). Importantly, there were repeat-associated differences in the neurons' ability to fire action potentials, either spontaneously or after current injection. In the HD180i.5/7 clones, no spontaneously firing neurons could be detected by 2 weeks of differentiation and there was no cell survival by 3 weeks of differentiation, suggesting a gradual dying off of cells over time (Table S4). This was in contrast to the other lines, which continued to express inward and outward currents and fire action potentials, all with similar magnitudes, and showed no increase in cell death at 3 weeks (Table S4). This acute cell death phenotype of the HD180 clones was reproduced by other consortium members using cell imaging and cleaved caspase 3 quantification (Figures 3H and 3I).

HD NSCs Generate Forebrain Cell Types and DARPP-32-Positive Neurons

To further pattern NSCs toward a striatal fate, we modified a published long differentiation protocol with stepwise differentiation in defined media over a period of 72 days (Figure 1C; Aubry et al., 2008). Using this protocol, which included more growth factors and the plating of cell clusters rather than dissociated cells, the widespread cell death phenotype seen for the HD180 line at 3 weeks using the short differentiation protocol was avoided. The expression of both neural and striatal-specific genes gradually increased over time in all lines with no obvious disease-specific differences (Figure 4A and S4). In addition, western blotting showed robust increases in cytoplasmic DARPP-32 protein in differentiated cultures of the HD109i.1 line compared to NSCs (Figure 4B). Together these data suggest that the HD NSCs were capable of producing neurons with a striatal phenotype. We next used immunocytochemistry (ICC) to visualize the developing striatal neurons (Figures 4C and 4D). Up to 10% of the cells from all lines were βIII-Tubulin- or Map2a/b-expressing neurons, and up to 5% were DARPP-32/Bcl11B positive, but variation between cultures and lines after the long, complex differentiation was too large to determine statistical differences between HD and control samples at a single time point. There was also some variability in gene expression at the endpoint of differentiation among three HD and two control samples (Figure 4E), in contrast to the similarities seen between lines at the NSC stage (Figure 1I). Interestingly, in the HD NSCs patterned toward a striatal fate, the majority of genes showed increased expression relative to controls (Figure 4E and S4). Key pathways affected in HD were identified with IPA, including those involved in proliferation, signaling, and cellular assembly (Table 1).

CAG-repeat-expansion-associated Phenotypes in Neural Cultures Derived from HD NSCs

We next asked whether HD NSCs patterned toward a striatal fate had an increased risk of dying over time by using the powerful approach of tracking live cells in longitudinal studies. Differentiated HD NSCs (long protocol) were transfected with a fluorescent reporter and followed with automated imaging and a longitudinal analysis system (Arrasate and Finkbeiner, 2005). The tracked cells that were frequently seen to die in these experiments often had morphological features of neurons, including tapering dendrite-like processes and thin axon-like processes extending hundreds of microns and tipped with growth cones (Figure 5A). To further confirm the identity of tracked live cells, separate cultures were fixed and cells with very similar morphologies were shown to express Map2a/b (Figure S5). By imaging labeled cells with neuronal-like morphology over time, we established that the cumulative risk of death was significantly higher for the HD180i.5 and HD60i.4 lines than the HD33i.8 line (Figure 5B). This is likely due to the expression of expanded CAGs in these lines, and indeed we showed that overexpressing 134 CAG repeats in the control HD33i.8 line led to an increased risk of death, similar to that seen in the HD180i.7 line (Figure 5C).

BDNF is reduced in HD patients, and may be connected with striatal degeneration (Zuccato and Cattaneo, 2009). In order to establish whether the HD lines may be sensitive to BDNF, we removed it from the medium and tracked cells over time. Following BDNF withdrawal, there was a higher cumulative risk of death in the HD180i.7 cells than the HD33i.8 cells (Figure 5D). Complementary studies using a nuclear condensation assay confirmed that another HD line (HD109i.1) and an additional clone (HD180i.5) also showed significantly greater amounts of cell death following BDNF withdrawal from the media than the HD33i.8 control line (Figure 5E). We also found a robust and significant CAG-associated increase in caspase 3/7 activity upon BDNF withdrawal, across multiple clones of the HD180i line, although the HD60 line showed a more variable clonal response (Figure 5F). Interestingly, the addition of four times the normal concentration of BDNF to the HD180.7 cultures

(F) Western blots of polyglutamine expression in iPSC-derived NSCs using the IC2 antibody demonstrate mutant HTT with expanded repeats in the HD-derived lines.
(G) Representative image of an NSC sphere demonstrating the section sampled for (H).
(H) HD iPSC-derived NSCs can be expanded as spherical aggregates in a self-renewing condition. ICC on cryosections of NSC aggregates demonstrated a consistent expression of the neural progenitor markers PAX6 and nestin in the three lines.
(I) Hierarchical clustering of the top 1,601 genes from NSCs is represented by the vertical bars (yellow for HD and green for control). The data set shows that HD and control NSC lines are separated into two clusters, confirming the differential expression of these genes into the two categories.

Table 1. Categorization of Significantly Differentially Expressed Genes by IPA

	Categories	Genes
HD versus control NSCs	cell signaling, organismal development, genetic disorder	**AGTR2**, BAI3, **CALCRL**, **CCKAR**, **CD97**, CELSR1, CELSR2, CELSR3, **CMKLR1**, **CYSLTR1**, **FZD1**, FZD3, **FZD4**, FZD7, **FZD8**, **GPR124**, **GPR155**, GPR160, **GPR174**, GPR19, **GPR37**, GPR63, **GPR64**, GPR98, GRM3, HRH2, HTR1D, **HTR2A**, **LGR5**, **LPAR5**, **NMUR2**, **NPY1R**, OPN1SW, **P2RY10**
	cell cycle, cancer, cellular assembly and organization	AASS, **ABCA8**, **AGTR1**, **ARHGAP18**, **CDKN2A**, **CYGB**, **EMILIN1**, **EYA4**, F11R, **F2RL2**, HIST1H3A, **IFI16**, **IFI30**, **IFI44**, IGSF5, **IRF6**, JAM2, **MFSD1**, NAP1L2, **NIPAL2**, **NMI**, NUAK2, ONECUT1, PMEL, SLC1A3, **SP110**, **SP140L**, **TBX2**, **TMEM173**, TMEM62, TMOD2, UCHL1
	connective tissue disorders, genetic disorder, dermatological diseases and conditions	**CD44**, **CHI3L1**, COCH, **COL12A1**, **COL15A1**, **COL16A1**, **COL19A1**, **COL1A1**, **COL1A2**, **COL21A1**, **COL24A1**, **COL25A1**, **COL3A1**, **COL4A1**, **COL4A2**, COL4A6, **COL5A1**, **COL6A1**, **COL6A2**, **COL6A3**, **COL6A6**, **COL8A1**, **DDR2**, HAPLN1, **ITGA10**, **ITGA11**, **MMP13**, **MMP2**, **MMP9**, PSAT1, **TIMP2**
	tissue development, embryonic development, cellular development	ALX4, BACH2, CAMK2N1, **DES**, **DLK1**, **DLX1**, **EPHA3**, **EPHA5**, **EPHA7**, EPHB1, **FOSL2**, GBX2, **GJB2**, **HOXB13**, **ISL1**, **KLF4**, **KLF5**, KLRG1, **LHX2**, **MAFB**, MME, MST4, NUAK1, PAX6, PTPN13, PTPRF, SALL1, SOX2, **SYNC**, **SYNM**
	gene expression, cellular movement, nervous system development and function	ABCG2, **AHNAK**, **AHR**, APBB2, **CSRP1**, **DYSF**, **EGFR**, EMX2, **ERRFI1**, **FABP3**, FABP7, GRB14, **LRRFIP1**, **MATN2**, MYOF, **NFIA**, **NFIB**, **NFIC**, **NFIX**, **OLFM1**, PIR, **POU4F1**, **RIN2**, **SEPP1**, **SPARCL1**, TFAP2C, **TLE2**, **UBASH3B**, **UTY**
Long CAG repeat versus control NSCs	neurological disease	**CAMK4**, **CHRM2**, GABRB3, **GJB6**, GLRB, **HTR2A**, **LIFR**, **PDP1**, **PLCB1**, SLC1A6, **SMAD6**, SNAP25
	axonal guidance signaling	**EPHA3**, EPHB1, **FZD1**, PAK1, PIK3C2B, **PLCB1**, PRKAG2, **RAC2**, **SEMA3E**, SEMA4D, **VEGFA**, WNT8A
Medium CAG repeat versus control NSCs	calcium signaling	**TNNT1**, CHRFAM7A, **MYH8**, **CREB5**, GRIA4, **RYR1**, **ACTC1**, **GRIK1**, **TP63**, **TRDN**, **CHRND**, PRKAR2B
	skeletal and muscular system development and function	**ACTN2**, **ANK2**, **CACNA1S**, CALCR, **CHRND**, ITGA2, MAP2K6, **MYBPC1**, **PLCE1**, **PSEN2**, **PTGS1**, **SGCA**
Long CAG repeat versus medium long HD	genetic disorder	ARPP21, ATP2A1, DGKB, TNNC2
	calcium signaling	ATP2A1, CHRND, GRIN3A, MYH3, TNNC2, TNNT2
HD versus control striatal-like cells	cellular growth and proliferation, cellular assembly and organization, cellular function and maintenance	**AHNAK**, **AK1**, **ASS1**, **BICC1**, **CCDC80**, **CCNE2**, **CSF1**, **CTSH**, **CYTL1**, DAAM1, EGF, **ERBB2**, **EXO1**, **FN1**, **FRRS1**, **GLIPR1**, **HGF**, **IGF1**, IRX1, **LPCAT3**, **MAN1A1**, MYEF2, **NEK3**, **NPNT**, **PARVA**, **PTPRG**, **STAG1**, **SUPT6H**, **TBC1D8**, **TP53**, **TSTA3**
	cell-to-cell signaling and interaction, connective tissue development and function, lipid metabolism	**CDCP1**, **COL14A1**, **CTSA**, **DCN**, **EFEMP2**, **ELN**, **EMILIN1**, **EMILIN2**, **FBLN1**, **FGF5**, **FKBP10**, **GLB1**, **HSPG2**, **MDK**, **MFAP2**, **MRC2**, **NEU1**, **NID2**, **PLA2G2A**, **PLSCR4**, **PPFIBP1**, **PTGIS**, **S100A4**, **SDC2**, **SDC4**, **SERPINA3**, **TPD52L1**
	tissue development, embryonic development, organ development	**ADAMTS12**, **ADAMTS9**, **ALDH1A3**, **AXL**, **B4GALT1**, **C1R**, **CASP12**, **CFB**, **CFH**, **COMP**, **DLK1**, **DOK5**, **EDA**, **EPHB4**, FABP6, **FOXF1**, **GREM1**, **GRN**, **HBP1**, **NMRAL1**, **PRDX4**, **RARG**, **RTKN**, **SRPX**, **TENC1**, **TNFAIP8**
	connective tissue disorders, genetic disorder, dermatological diseases and conditions	**ANTXR1**, **ANTXR2**, **COL11A1**, **COL12A1**, **COL16A1**, **COL1A1**, **COL1A2**, **COL21A1**, **COL25A1**, **COL27A1**, **COL3A1**, **COL4A1**, **COL5A1**, **COL5A2**, **COL6A2**, **COL6A3**, **COL6A6**, **CREB3L1**, **CTSK**, **DDR2**, **ITGA11**, **MMP13**, **MMP16**, **MMP2**, **PCOLCE**, **THBS1**
	cellular assembly and organization, cellular function and maintenance, cellular movement	**ANGPTL4**, **AP3B1**, **ARHGAP6**, **CAST**, **DAB2**, DLL1, **ERF**, **FURIN**, **GORASP2**, **LAMA2**, **LAMB1**, **MMP14**, PACRG, PCLO, **PLAGL1**, **PTPRN**, PTPRN2, RASA4, **RPSA**, **S100A11**, **SNTB2**, **SNX9**, **SYT4**, **TMEM119**, **UTRN**

HD versus control NSC samples or HD versus control striatal-like samples were analyzed and organized by IPA into functional categories and networks. Genes from these groupings are shown. Genes in bold represent significantly increased gene expression and nonbolded genes represent significantly decreased gene expression. Only the most highly ranked groupings were selected. The top subsection shows the top ranked categories for all 1,601 differentially expressed genes in HD versus control NSCs. Three center subsections depicting representative genes from the top two categories are shown. Long CAG repeat versus control NSCs contains changes between only the HD180 and HD109 lines, and not the HD60 line, compared to controls. Medium CAG repeat versus control NSCs contains changes between HD60 and control. Long CAG repeat versus medium CAG repeat contains genes from an analysis of HD180 and HD109 versus HD60. The representative genes in the subsections are also in the list of HD versus control NSCs genes (top). The fact that there are such genes explains why subtle differences can be seen in the hierarchical clustering/heatmap between these lines (Figure 1I). The bottom section shows the top five IPA categories for differentially expressed HD versus control striatal-like cells.

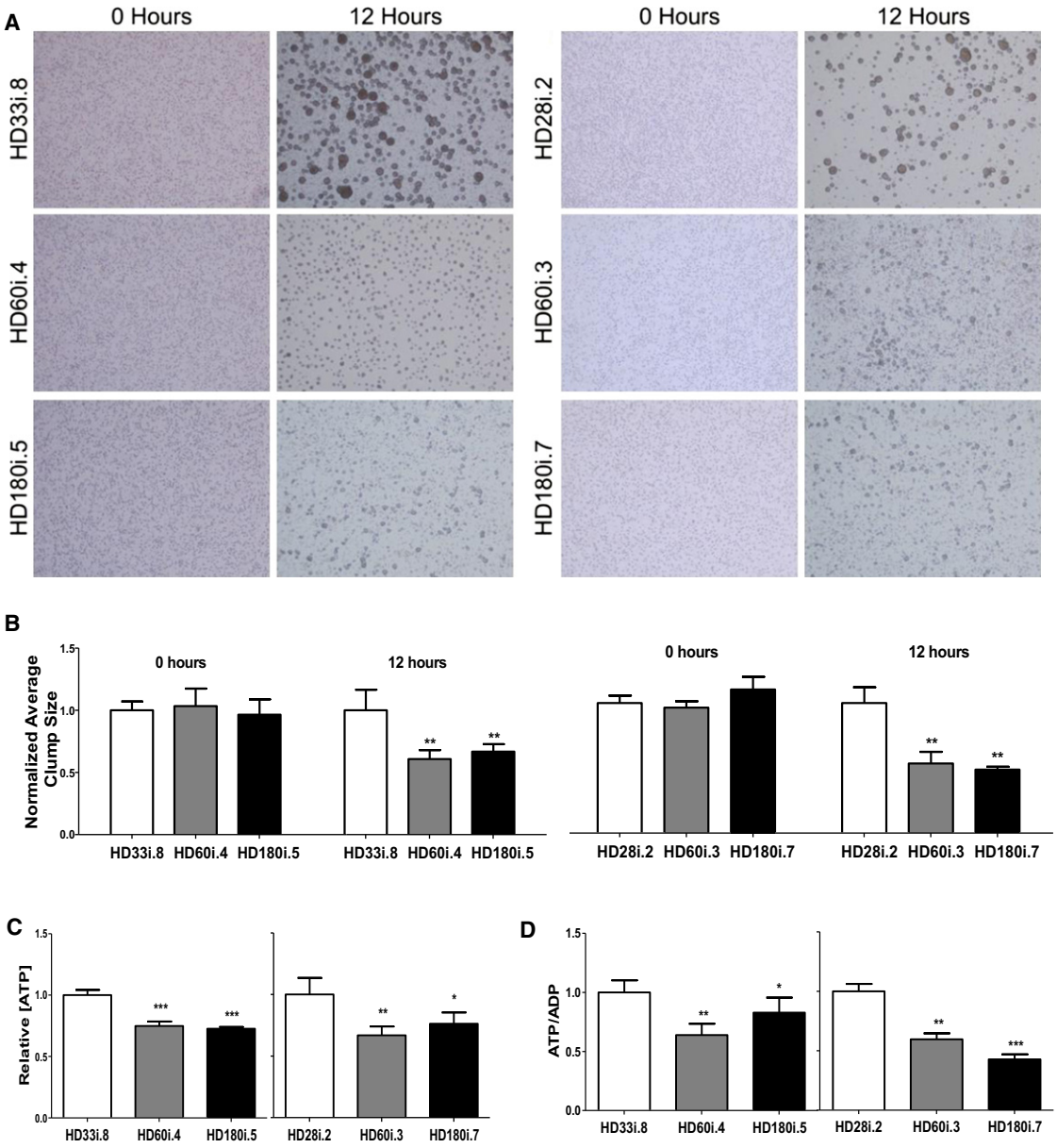

Figure 2. NPCs with Expanded CAG Alleles Exhibit Altered Cell-Cell Adhesion and Energetics

(A) Representative micrographs demonstrating similar dispersion of NPCs at time 0, for all genotypes, and cell-cell clusters formed at 12 hr, which were larger with shorter CAG alleles, compared to NPCs with longer CAG alleles.

(B) Quantitative analysis of average NPC cluster size at time 0 and 12 hr, showing a significant difference at the 12 hr time point between the shorter CAG (HD33i.8 and HD28i.2) and the longer CAG (HD60i.4, HD60i.3, HD180i.5, and HD180i.7) alleles, consistent with decreased cell adhesion.

(C) The relative intracellular [ATP] values were decreased in NPCs with longer CAG alleles (HD60i.4, HD60i.3, HD180i.5, and HD180i.7) compared to those with shorter CAG alleles (HD33i.8 and HD28i.2).

(D) The relative intracellular [ATP/ADP] ratio for the longer CAG alleles (HD60i.3, HD60i.4, HD180i.5, and HD180i.7) was significantly decreased compared to NPCs with shorter CAG alleles (HD33i.8 and HD28i.2).

All graphs show plotted cell values normalized to the low CAG allele controls. Error bars indicate SD; *$p < 0.05$, **$p < 0.01$, and ***$p < 0.001$.

significantly reduced the cumulative death, although not to control levels (Figure 5G).

We wanted to establish whether exposing HD cells to excitotoxic stress using glutamate could bring out a more robust phenotype, as has been shown previously using hydrogen peroxide on dopamine neurons derived from Parkinson's disease iPSCs (Nguyen et al., 2011). Using the short differentiation protocol, we first confirmed that increases in $[Ca^{2+}]_i$ were evoked by extracellular KCl, γ-aminobutyric acid, L-glutamate/L-glycine, N-methyl-D-aspartic acid, kainate, and α-amino-3-hydroxyl-5-methyl-4-isoxazole-propionate (AMPA), demonstrating that $GABA_A$ and the three subtypes of ionotropic

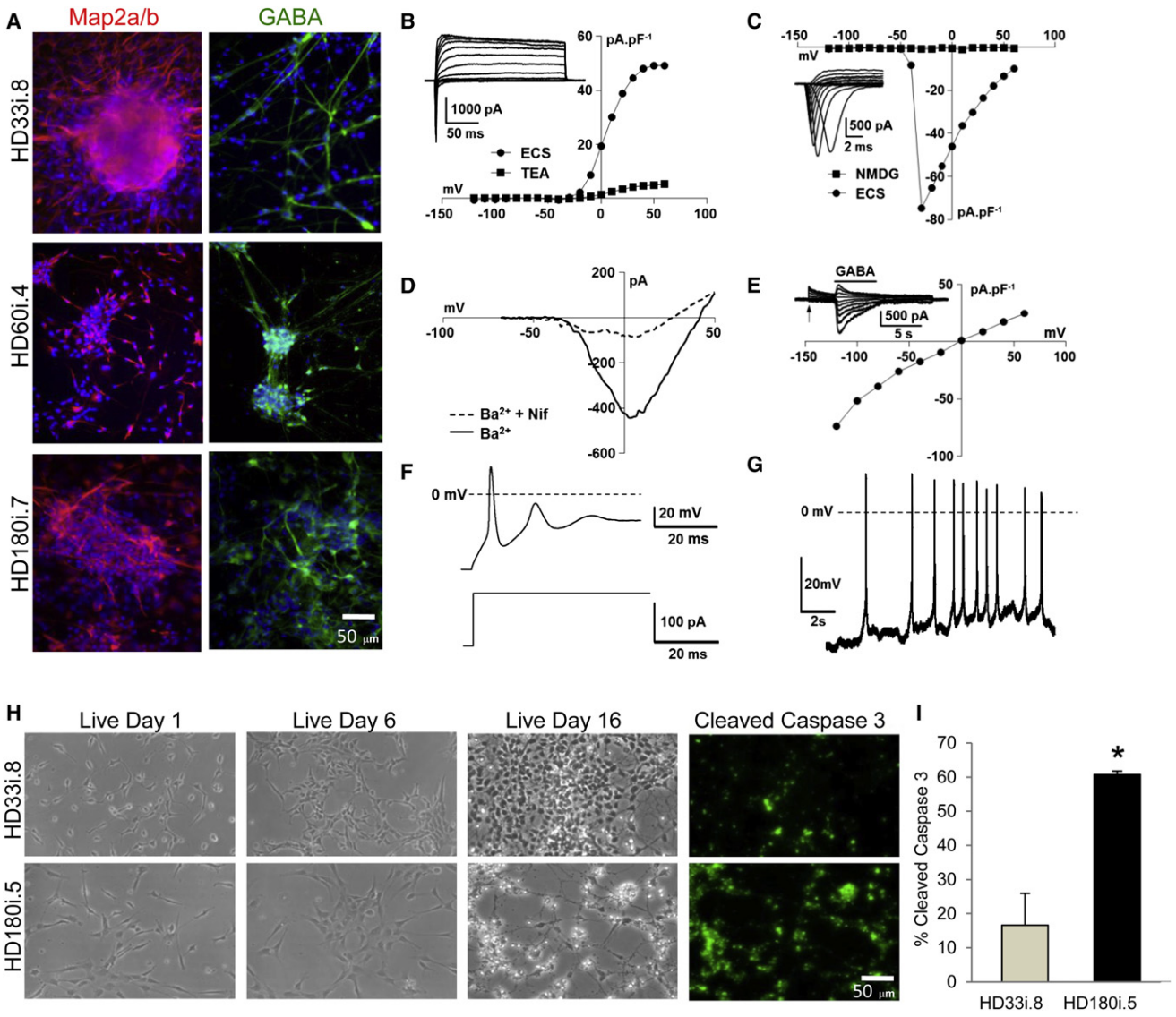

Figure 3. iPSCs Can Be Differentiated into Mature, Electrophysiologically Active Neurons Susceptible to Glutamate Toxicity

(A) HD180i, HD60i, and HD33i lines differentiated for 14 days were positive for MAP2a/b and GABA (scale bar, 50 μm).

(B) Current density (pA.pF^{-1}) versus voltage (mV) relationships for the outward, voltage-activated currents of the exemplar conventional whole-cell recording shown in the inset in normal extracellular solution (ECS) and after iso-osmotic addition of 20 mM tetraethylammonium chloride (TEA). Holding potential = −70 mV.

(C) Current density (pA.pF^{-1}) versus voltage (mV) relationships for the inward, voltage-activated currents of the same cell as in (B) in the presence of ECS and after iso-osmotic replacement of Na^+ with N-methyl D glutamine (NMDG). The exemplar family of Na^+ currents in the inset was recorded in the presence of 20 mM TEA and is displayed on a fast time base. Holding potential = −70 mV.

(D) Current (pA) versus voltage (mV) relationships, evoked using a voltage-ramp protocol, for currents carried by Ba^{2+} (27 mM, iso-osmotic replacement of NaCl, Ba^{2+}) in the absence and presence of 2 mM of the L-type Ca^{2+} channel blocker, nifedipine (Ba^{2+} + Nif). Holding potential = −110 mV.

(E) Current density (pA.pF^{-1}) versus voltage (mV) relationship for Cl^- currents activated by 300 mM GABA. The inset shows a family of GABA-activated currents recorded at the voltages shown in the main panel; GABA application is indicated by the bar above the traces shown and the voltage was stepped from −60 mV to the voltages indicated in the main panel at the point indicated by the arrow. Holding potential = −70 mV.

(F) Typical evoked action potential (upper trace) recorded under current-clamp in the conventional whole-cell patch-clamp configuration during the current injection shown in the lower trace (from 0 to + 120 pA).

(G) Example of spontaneous action potential activity recorded under current-clamp (I = 0 mV) in the conventional whole-cell patch-camp configuration.

(H and I) Staining for cleaved caspase 3 revealed increased apoptotic death in the HD180i.5 line over time compared with the control line HD33i.8 ($p < 0.05$, Student's t-test and error bars are SEM).

glutamate receptors were expressed in these cultures (Figure S6). Then, cultures were exposed to 20 s pulses of glutamate and were examined using fura-2 ratiometric imaging of intracellular Ca^{2+} concentration ($[Ca^{2+}]_i$). Interestingly, using this assay there was a clear CAG-repeat-expansion-associated phenotype in Ca^{2+} handling after 20 s pulses with glutamate (Figure 6A).

Because in HD there is evidence for chronic, elevated exposure of cells to glutamate (Behrens et al., 2002; Faideau et al., 2010), we also examined cells differentiated under chronic exposure to pathological levels of glutamate (150 μM), which significantly exacerbated the Ca^{2+} dyshomeostatis in the HD180i lines (Figure 6B).

We next assessed the effects of glutamate pulsing by using the long differentiation protocol. Staining and quantification of TUNEL-positive nuclei demonstrated that multiple 30 min glutamate pulses led to an increased level of cell death in the HD cultures (Figures 6C and 6D). While the HD33i line showed apparent increases in death after pulsing, it also had a higher basal level of cell death (40% versus 20%) and so this increased death did not reach significance when compared to basal levels. While repeated glutamate pulsing has previously been shown to induce aggregation of the polyQ-expanded protein ATXN3 in SCA3 iPSC lines (Koch et al., 2011), we did not see aggregation of the expanded HTT protein by ICC in these cultures (data not shown). Finally, we evaluated the effects of other HD-related toxic stressors on cell survival. Both H_2O_2 (oxidative stress) and 3-methyladenine (3-MA) (autophagy inhibition), but not lactacystin, led to an increased amount of cell death in the HD lines when compared to controls (Figures 6E and 6F). Together these data suggest that the risk of death for HD iPSC differentiated cultures was far greater than that of the control cultures. This was evident through multiple means of stressing the HD-derived cells, including the withdrawal of trophic support, pulsing with glutamate, or the addition of cellular stressors.

DISCUSSION

This study characterizes a set of CAG-repeat-expansion-associated phenotypes in neural cells derived from HD iPSC lines. A unique aspect of the current report was that we worked as a consortium, using the same set of lines in a wide range of cellular assays. HD is an ideal disorder for exploring the utility of iPSCs for disease modeling because it is caused by a single gene and there is a strong correlation between the length of the expanded CAG repeat and the age of disease onset (Consortium, 1993; Stine et al., 1993). In addition, there is a weaker, though still highly significant correlation between the length of the expanded repeat and rate of progression of some clinical phenotypes (e.g., motor and cognitive disorder), though not others (e.g., emotional disorders) (Rosenblatt et al., 2012). Interestingly, we found that in some assays, such as cellular aggregation, overall energy metabolism, and cumulative risk of death over time in the long differentiation protocol, both the HD60 and HD180 lines showed very similar pathological profiles that were significantly different from control lines. However, in other assays, such as cell survival in a short differentiation protocol, BDNF withdrawal, and glutamate toxicity, only the HD180 line (and, where tested, the 109 line) showed a robust phenotype. Finally, in one assay we developed based on calcium homeostasis following repeated glutamate pulsing, we saw a clear, repeat-dependent phenotype with a graded response across the HD33, HD60, and HD180 lines. The gene array studies also suggested a gradation of expression changes, particularly those that are differentially expressed in both the very long repeat lines (HD180 and HD109) and the more moderate length repeat line (HD60) compared to control lines, but there are also clear differences between the long and medium repeat lines within this group. Together these studies suggest that there are clear phenotypes associated with expanded CAG repeats, and that the choice of assay and exact tissue culture conditions will determine the extent of the phenotypic gradation with the length of the CAG expansion that can be detected.

The success of this model reflected the maintenance of the *HTT* CAG repeat expansion following reprogramming, stem cell expansion, and subsequent differentiation. The HD lines demonstrated only mild CAG repeat instability in culture, and the slight increase in repeat number with passaging for one of the longest CAG lines (HD109) may correspond to the somatic genomic CAG instability seen in tissues from HD patients (Shelbourne et al., 2007). As expected, we found expression of the mutant protein in these cultures, although no inclusion bodies were found in the cells before or after differentiation, or after the addition of cellular stressors, possibly reflecting the long period of time before inclusions develop in the human disease (Ross and Poirier, 2004). It is important to note that while HTT inclusions are pathognomonic in postmortem tissue, inclusion formation is not linked to HTT cell toxicity (Arrasate et al., 2004).

Alterations in gene transcription and protein expression are prominent in HD mouse models and human HD brain tissue (Ross and Thompson, 2006). In dividing HD NSCs, which had a very stable number of nestin-positive progenitors, we observed HD-related changes in expression of genes including SLC1A3 (Fan and Raymond, 2007), UCHL1 (Xu et al., 2009), EGFR (Lievens et al., 2005), and TRK receptors (Apostol et al., 2008; Zuccato et al., 2010), consistent with changes in human HD brain (Hodges et al., 2006) and HD transgenic mouse striatum (Luthi-Carter et al., 2000). Among the genes upregulated, GLB1, PLSCR4, PTGIS, and PLA2 have been implicated in lipid metabolism and membrane fluidity, with possible consequences for cell signaling and receptor function in HD (Karasinska and Hayden, 2011). Additional altered pathways were identified, including a network of G protein-coupled receptors, developmental genes such as PAX6, and matrix metalloproteinases, consistent with the involvement of this family of proteases in mutant HTT toxicity (Miller et al., 2010). The concordance of pathways and networks at RNA and protein levels further suggests a primary dysfunction of these systems in this model of HD. These results suggest that expanded CAG repeats were having a biological effect even at the NSC stage, and further analysis of these pathways may uncover factors that contribute to emerging HD pathology (Molero et al., 2009).

Following cell differentiation to a striatal-like phenotype, we found more genes with increased rather than decreased expression, as shown previously in studies of human HD striatum (Hodges et al., 2006). Genes upregulated in human tissue and differentiated HD iPSCs included p53, which is also upregulated in HD mice and may contribute to the cell death seen in this study and those of others (Bae et al., 2005); syndecan4, involved in recycling of lipids and cholesterol from degenerating terminals (Blain et al., 2004); HMG box protein 1, a tumor suppressor and transcription factor that accumulates in the Alzheimer's brain and may impair Aβ clearance (Takata et al., 2004); and SRPX, which contributes to language and cognitive

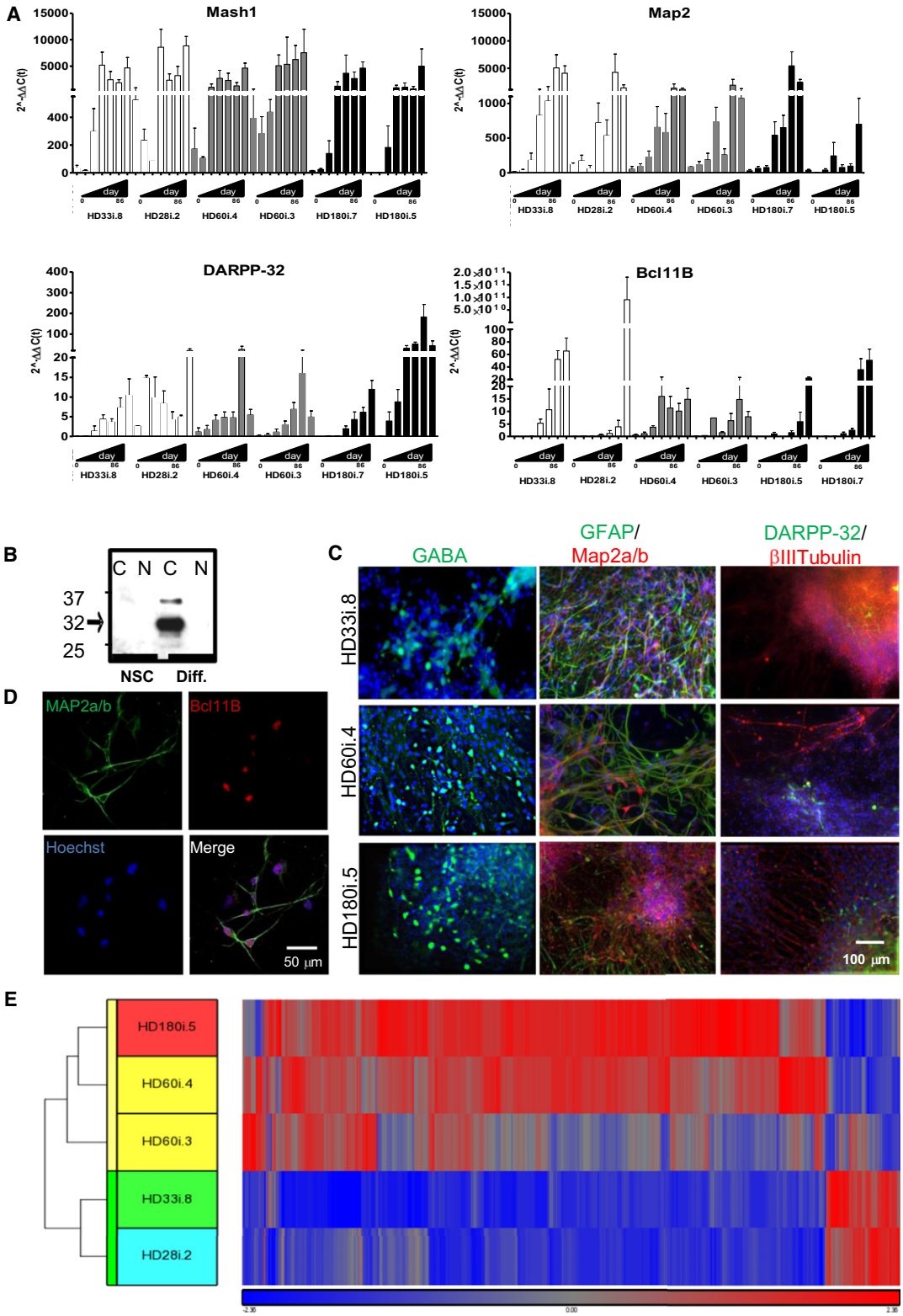

Figure 4. iPSCs Can Be Differentiated into a Striatal-like Phenotype

(A) qRT-PCR from day 0 (NSC stage) to 86 using the long differentiation protocol for HD180i.5/7, HD60i.3/4, and HD28i.2/HD33i.8 demonstrates that neural (Mash1), neuronal (MAP2), and striatal-specific (DARPP-32 and Bcl11B) genes upregulate over time. Error bars are SEM.

(B) Western blots for DARPP-32 in HD109i.1 NSCs and differentiated cells also show upregulation in the cytoplasmic (C) but not nuclear (N) fraction upon differentiation.

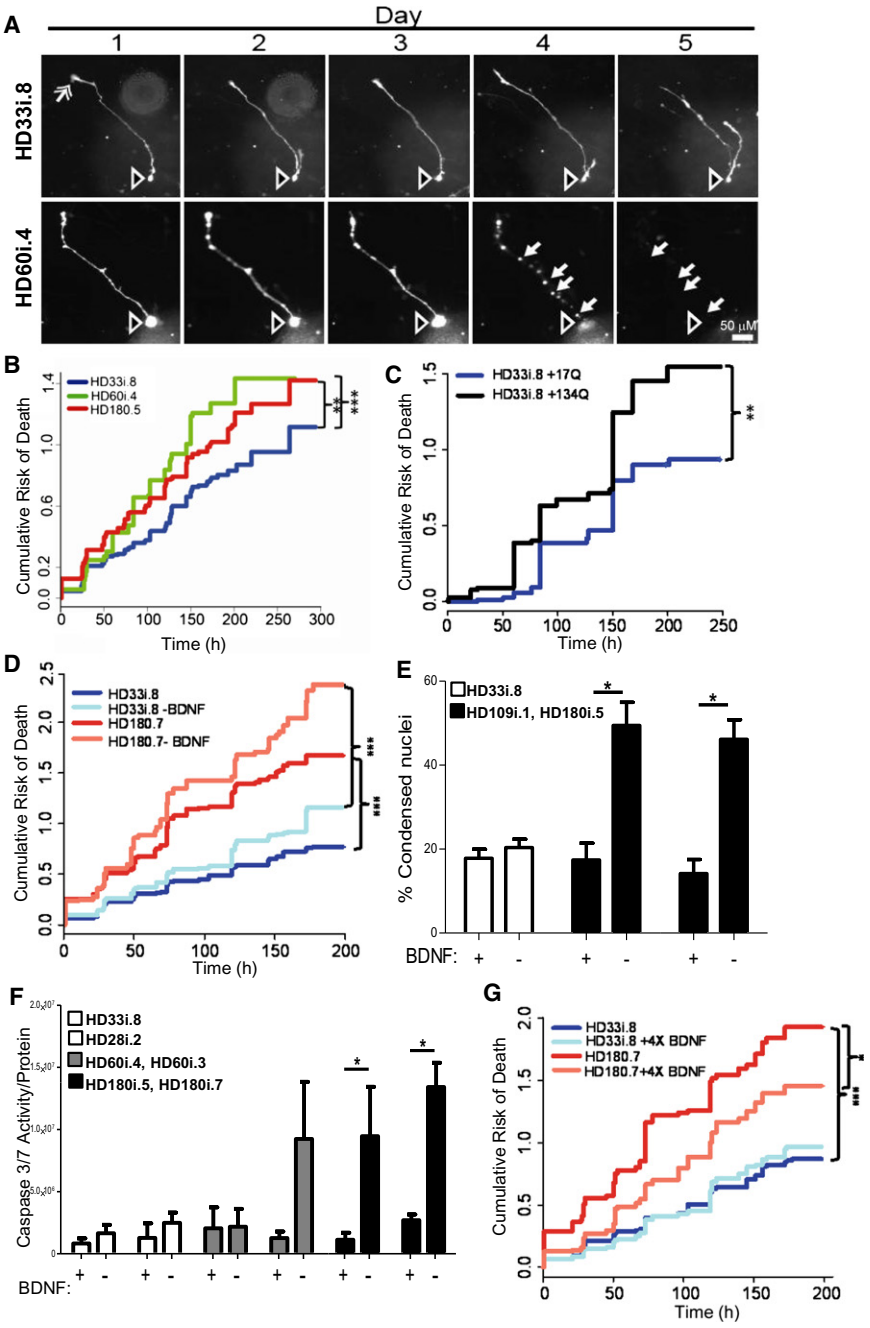

Figure 5. HD iPSCs Show Increased Risk of Death over Time in Culture and After Trophic Factor Withdrawal

(A) Examples from a time series of images of two differentiated cells at day 35 from the HD33i.8 and HD60i.4 lines. Often cell bodies (hollow arrow, top and bottom rows) extend 1–3 processes, which are tipped by structures resembling growth cones (solid arrow, upper row, day 1). Degeneration and cell death were evident (bottom row, compare days 3–5) from the blebbing and retraction of neurites (closed arrows) and the loss of the cell soma (open arrow). Scale bar, 50 μm.

(B) Kaplan-Meier analysis revealed that the cumulative risk of death was higher for the HD180i.5 (hazard ratio is 1.4, $p < 0.01$, n = 337 cells) and the HD60i.4 (hazard ratio is 1.5, $p < 0.001$, n = 164 cells) lines compared to the HD33i.8 (n = 248 cells) line. Total n = 750 cells; six experiments for HD60i.4, seven for HD180i.5, and eight for HD33i.8.

(C) The cumulative risk of death is significantly increased in HD33i.8 cells overexpressing (by plasmid transfection) 134 CAG repeats (94 cells) compared to cells overexpressing 17 CAG repeats (92 cells). $p < 0.01$, hazard ratio is 1.7, n = 2 experiments.

(D) The risk of death was significantly higher for the HD180i.7 line (195 cells) grown in BDNF compared to the HD33i.8 line (134 cells) grown in BDNF. Hazard ratio is 2.1 ($p < 0.001$). After BDNF removal, the risk of death was significantly greater for the HD180i.7 line (156 cells) compared to the HD33i.8 line (n = 191 cells); the hazard ratio is 2.56 ($p < 0.001$). Removal of BDNF did not significantly increase the risk of death for the HD33i.8 and HD180i.7 lines compared to the lines grown in BDNF; however, the increased risk of death for the HD180i.7 line after BDNF removal approached significance ($p = 0.08$, hazard ratio = 1.22, n = 4 experiments).

(E) BDNF was withdrawn for 48 hr, and cells were fixed and labeled with Hoechst. Quantifying condensed nuclei as a measure of cell toxicity showed that both HD109i.1 and HD180i.5 lines had significantly more cell death after BDNF withdrawal, whereas the HD33i.8 control line showed no change. ANOVA; *$p < 0.01$ and error bars are SEM.

(F) Quantifying caspase 3/7 after BDNF was withdrawn for 24 hr showed that both clones of the HD180i line demonstrated significant increases in caspase 3/7 activity. In addition to BDNF, dbcAMP and VPA were removed from the medium because they increase endogenous BDNF transcription (Pruunsild et al., 2011). Error bars are SEM. *$p < 0.05$ ANOVA

(G) Addition of 4× BDNF reduced the cumulative risk of death for HD180i.7. The risk of death is significantly less for the HD180i.7 line plus 4× BDNF (108 cells) compared to the HD180i.7 line alone (182 cells) ($p < 0.001$). The hazard ratio is 0.67. There is no difference in the cumulative risk of death between the HD33i.8 line (208 cells) that received 4× BDNF (156 cells; $p = 0.43$). The hazard ratio is 1.06 (n = 4 experiments).

development (Royer et al., 2007). An advantage of this iPSC model is that gene expression changes in human neurons can be identified over time during the degeneration process and at specific stages of neuronal differentiation to illuminate pathogenic mechanisms, in contrast to gene expression studies done only in end-stage postmortem human HD brain tissue.

(C) HD180i, HD60i, and HD33i cells differentiated for 56 days expressed βIII-Tubulin (immature neuron), DARPP-32 (striatal), GFAP (glia), MAP2a/b (mature neuron), and GABA (GABAergic neuron). Nuclei are stained with Hoechst.

(D) HD109i.1 cells can be differentiated into mature, striatal-like neurons that express MAP2a/b and Bcl11B.

(E) Hierarchical clustering of the top 787 genes from striatal-like cells is represented by the vertical bars (yellow for HD and green for control). The data set shows that most genes are upregulated in the HD lines and that they can be separated into two defined clusters.

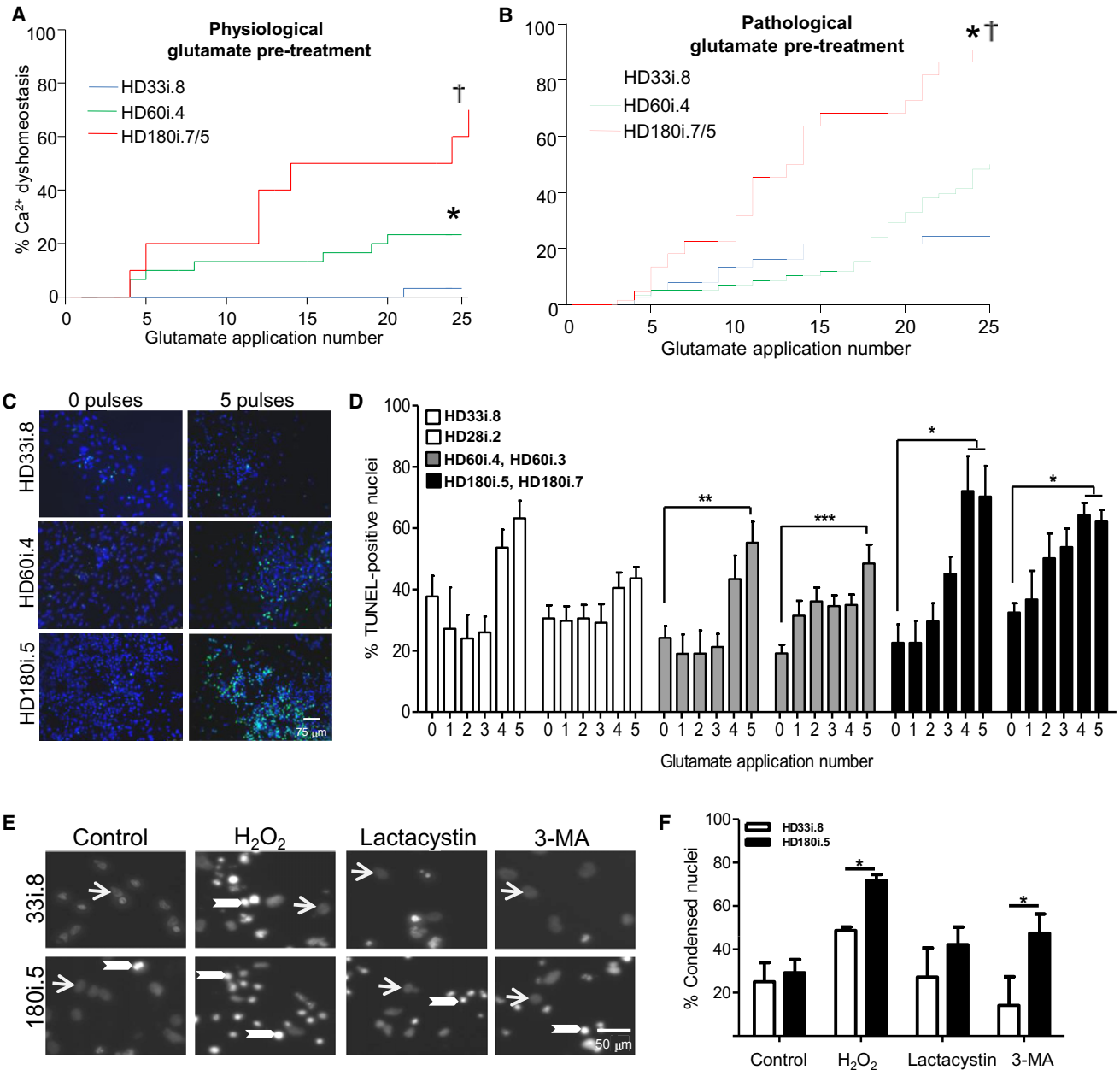

Figure 6. HD iPSCs Have Increased Vulnerability to Stress and Toxicity

(A) Using the short differentiation protocol, Ca^{2+} dysfunction was significantly elevated in the HD lines compared to the HD33i.8 line (*$p < 0.02$; †$p < 0.001$).

(B) As in (A), except after a 14 day chronic pretreatment with pathological glutamate (150 μM). Significantly different from HD33i.8, *$p < 0.005$; HD60i.4, †$p < 0.0001$.

(C) Images demonstrate TUNEL-positive nuclei (green) and total nuclei (blue) in HD and control lines after exposure to either no glutamate or five glutamate pulses.

(D) HD iPSCs were differentiated for 56 days before exposure to repeated 30 min pulses (0–5) of 50 μM glutamate. Cells were allowed to rest 24 hr before cell death was analyzed. Compared to the zero glutamate pulse condition, TUNEL staining was significantly increased in both clones of the HD180i line after four or five glutamate pulses and in both clones of the HD60i line after five glutamate pulses. The control lines showed no significant increase (one-way ANOVA with Bonferroni posttest. Error bars are SEM. *$p < 0.05$, **$p < 0.01$, ***$p < 0.001$ ANOVA Error bars are SEM and *$p < 0.05$, **$p < 0.01$, ***$p < 0.001$.) after five pulses.

(E) Images demonstrate noncondensed nuclei (arrows) and bright condensed nuclei (arrowheads) in HD180i.5 and HD33i.8 differentiated iPSCs in either non-treated media or media treated with 300 μM H_2O_2, 10 μM lactacystin, or 5 mM 3-MA.

(F) Nuclear condensation assay shows enhanced toxicity of HD180i.5 cells compared to control HD33i.8 cells upon treatment with H_2O_2 or 3-MA. *$p < 0.05$ and error bars represent SEM.

A number of dominant, CAG-repeat-expansion-associated biochemical and cell biological phenotypes, such as altered cell adhesion and altered energetics, have been observed in murine *Hdh* CAG knockin ESCs and derived immortalized lines (Ginés et al., 2010; Jacobsen et al., 2011). Neural progenitors derived from the HD60i and HD180i NSC lines were found to

undergo less aggregation upon plating, and showed significantly reduced ATP levels compared to control lines. This suggests disruptions of cell adhesion and energy metabolism, which may alter the cells' ability to survive and differentiate appropriately. This was reflected by a gradual reduction in the number of neurons that could generate spontaneous and induced action potentials over time in the HD lines, and ultimately cell death by 3 weeks of differentiation in the HD180i cultures. Thus, our studies showed that under specific culture conditions, there was a severe phenotype associated with endogenous levels of mutant HTT expression.

Using a longer differentiation protocol that included the addition of multiple growth factors to direct the cells toward a striatal lineage (Aubry et al., 2008), it was possible to avoid the acute stress-related neural cell death seen in the HD NSC lines, again reinforcing the idea of stress being a key component of these in vitro models of disease. A very sensitive single-cell time-lapse assay (Arrasate et al., 2004) showed conclusively that cells within the HD60i and HD180i lines had a significantly greater cumulative risk of death than those in control lines. Furthermore, a similar cell death pattern in control lines could be seen due to overexpression of mutant, but not normal, HTT. To uncover further phenotypes in cultures at single time points may require stressors to the system, as shown in iPSC models of Parkinson's disease and SCA3 (Mattis and Svendsen, 2011; Seibler et al., 2011). We found clear CAG-repeat-expansion-associated differences in the vulnerability of cells to the addition of exogenous stressors, such as H_2O_2 or 3-MA, or the repetitive exposure to glutamate. This is of interest in light of studies showing that HD may be associated with increased reactive oxygen species (Túnez et al., 2011). Withdrawal of BDNF from the medium also revealed a CAG expansion-associated toxic phenotype, based on the time-lapse assay, nuclear condensation assays, and caspase activation. There is a long literature on the role of BDNF in HD pathogenesis in relation to striatal neuron vulnerability (Zuccato and Cattaneo, 2009), as well as reported toxicity in response to BDNF withdrawal in a single HD iPSC line (Zhang et al., 2010). Our new data further support a central role of BDNF in HD. It will be of interest to test if there is preferential cell toxicity in neurons expressing striatal markers, as contrasted with other neurons in the culture. This kind of preferential toxicity was seen for dopamine neurons in a recent report on iPSCs derived from a patient with a LRRK2 mutation (Nguyen et al., 2011). However, in HD, unlike in Parkinson's disease, there is widespread neuronal dysfunction and death, especially in cases with long repeats, so cell toxicity may not be limited purely to striatal neurons.

Our study is notable for detecting clear, CAG-repeat-expansion-associated phenotypes, including cell toxicity, as would be expected for a neurodegenerative disease such as HD. We observed three variations on the relationship between phenotypes and the length of the CAG expansion in cells differentiated from HD iPSCs compared to controls. Some phenotypes were present in the HD lines in a graded fashion that correlated with the length of the CAG expansion. Others were only found in lines with the longest CAG expansion. Still others were present to a similar extent in lines with HD-associated CAG expansions of any length. The ability to detect a relationship between the length of the CAG expansion and dysfunction induced by mHTT will likely depend on a number of factors including the sensitivity and dynamic range of a particular assay and the cell type being studied. Our data would also be consistent with a model of HD pathogenesis in which the number of affected pathways and, in some cases, the extent of their dysfunction varies with the length of the CAG expansion. The CAG dependence of neurodegeneration could therefore be an emergent property of the cumulative effect of a multifarious network of pathways affected by mHTT.

In conclusion, we have developed and characterized an iPSC model of HD that includes multiple lines, clones, and repeat lengths. Future experiments using an allelic series of cell lines with a range of expanded repeat lengths will help define the CAG-repeat-expansion-associated dependence of different phenotypes. The utility of this model system includes elucidation of HD cellular pathogenesis, development of HD-specific biomarkers, and ultimately screening for small molecule or other therapeutic interventions.

EXPERIMENTAL PROCEDURES

Generation and Characterization of iPSC Lines

Human fibroblast lines were obtained from two HD patients with expanded CAG alleles of 60 and 180 repeats and from one non-HD sister of the former with 33 repeat CAG alleles (Table S1 and Table S2). Reprogramming was conducted by lentiviral transduction of six transcription factors (*Oct4*, *Sox2*, *Klf4*, *cMyc*, *Nanog*, and *Lin28*) as previously described (Yu et al., 2007). A number of clonal colonies with iPSC morphology (Figure 1A) were expanded into stable iPSC lines named HD33i.x, HD60i.x, and HD180i.x, where "x" defines the clone number. Additional iPSC lines were generated from patient fibroblast samples collected by consortium members (Table 1; HD109 and HD21), using retroviral transduction and maintenance of iPSC colonies as described in Takahashi et al. (2007). A previously generated control line (HD28i.2) was also used in some experiments (WT4.2; Ebert et al., 2009). Finally, HD lines have been generated, but not yet characterized, using non-integrating methods (Yu et al., 2009). Karyotyping and teratoma formation were performed, and are described further in the Supplemental Experimental Procedures.

Generation of iPSC-Derived NSC Lines

NSC lines were generated by treating iPSC colonies with collagenase (1 mg/ml, GIBCO) and lifting them from the feeder layers directly into Stemline medium (Sigma) supplemented with 100 ng/ml basic FGF (Chemicon), 100 ng/ml EGF (Chemicon), and 5 μg/ml heparin (Sigma) in polyhema-coated flasks to prevent attachment. iPSC-derived NSCs were expanded as spherical aggregates and passaged weekly with a chopping technique (Svendsen et al., 1998).

Neural Differentiation from NSCs

A short differentiation protocol with NSCs plated onto laminin-coated coverslips was used for some experiments (Figure 1C, see Supplemental Experimental Procedures). In addition, a long differentiation protocol was used based on a protocol from Aubry et al. (2008) (Figure 1C). Growth medium containing EGF/FGF was removed from NSCs, and cells were plated on laminin or allowed to aggregate for 5 days in NIM (1% N_2 in DMEM:F12). BDNF (20 ng/ml; Peprotech 450-02) was then added for 2 days. The medium was then supplemented for 21 days with BDNF, rhShh (200 ng/ml; R&D 1845-SH), and Dkk1 (100 ng/ml; R&D 1096-DK-010). The rest of the differentiation was then completed in NIM with BDNF, dibutyryl cyclic AMP (dbcAMP, 0.5 mM; Sigma D0260) and valproic acid (VPA, 0.5 mM; Sigma P4546). Medium was half-changed twice per week or as needed. If cells were differentiated as aggregates, they were plated on day 42.

RNA Isolation and Quantitative Reverse-Transcriptase PCR Analysis

Total RNA was isolated using the RNeasy Mini Kit (QIAGEN) and digested by DNase I (RQ1 DNase, Promega). Complementary DNA was generated from

0.5–2 μg total RNA using a Reverse Transcript System (Promega A3500 or Invitrogen). qRT-PCR and primer sequences are described in the Supplemental Experimental Procedures.

Immunocytochemistry

Cells were fixed in 4% paraformaldehyde (PFA) at room temperature, rinsed with PBS, and permeabilized with 5% normal goat and/or donkey serum containing 0.2% Triton X-100 for 30 min at room temperature. Cells were then labeled with primary antibodies (listed in the Supplemental Experimental Procedures) for 60 min at room temperature or overnight at 4°C, and then the appropriate fluorescently tagged secondary antibodies for 60 min at room temperature. Hoechst nuclear dye was used to label nuclei. Cells were counted using stereological software (stereoinvestigator).

Western Blotting

Western blotting was performed per manufacturer recommendations. The HTT-specific antibody 2166 (Millipore) was used to detect HTT protein in the control and HD lines. The expanded polyglutamine-specific antibody IC2 (Chemicon) was used to detect mutant HTT in the HD lines.

BDNF Withdrawal

Cells were differentiated toward a striatal fate for 52–54 days and then transferred into basic NIM without BDNF, VPA, and dbcAMP for 48 hr. Cell death was measured by quantifying condensed nuclei (described in below assay). In addition, cells were differentiated toward a striatal fate for 42 days and then transferred into basic NIM, NIM plus 10 ng/ml BDNF/0.25 mM VPA/0.25 mM dbcAMP, NIM plus 20 ng/ml BDNF/0.5 mMVPA/0.5 mM dbcAMP, or NIM plus 20 ng/ml BDNF alone for 24 hr. Caspase 3/7 activity was measured using a Caspase-Glo 3/7 assay (see Supplemental Experimental Procedures). dbcAMP and VPA were removed from the medium in the above experiments because they increase endogenous BDNF transcription but are not critical for cell survival (Pruunsild et al., 2011).

Cell Stress and Toxicity Assays

To assess the effects of cellular stressors, differentiated iPSCs were treated with 3-MA (5 mM) for autophagy inhibition, lactacystin (10 μM) for proteasome inhibition, and hydrogen peroxide (H_2O_2, 300 μM) for oxidative stress. All reagents were purchased from Sigma. Cells were then fixed with 4% PFA, permeabilized with 0.3% Triton X-100, and stained with 0.4 μg/ml Hoechst 33342. Cell toxicity was assayed by quantifying condensed nuclei with the Volocity software (Perkin-Elmer) with the Zeiss Axiovert 200 microscope and is described further in the Supplemental Experimental Procedures. Cells were considered as nonviable when their Hoechst intensity was greater than 200% of the control intensity.

To assess the effects of cellular toxicity, cells were differentiated for 56 days and then treated with zero to five 30 min pulses of 50 μM glutamate (Sigma G1251) in DMEM:F12 1:1, with 30 min no-glutamate rests between pulsing. At the end of treatment, cells were maintained in conditioned media for 24 hr before fixation in 4% PFA. Effects of glutamate pulses were assessed by quantifying TUNEL incorporation per total Hoechst-stained nuclei, according to manufacturer recommendations (Promega DeadEndFluorometric TUNEL System, G3250). Effects of glutamate pulses were also assessed by measuring Ca^{2+} dyshomeostasis (see Supplemental Experimental Procedures).

Automated Survival Assays

Cells were transfected with reporter genes and then plated and imaged as described in Arrasate and Finkbeiner (2005), Arrasate et al. (2004), and our Supplemental Experimental Procedures.

Electrophysiology and Calcium Imaging

Details are given in the figure legends and the Supplemental Experimental Procedures.

Gene Expression Studies

Microarray experiments were performed using Affymetrix Human Gene 1.0 ST Arrays. RNA integrity was verified using a Bioanalyzer 2100 (Agilent) and processed at the UC Irvine Genomics High-Throughput Facility. Additional details are in the Supplemental Experimental Procedures.

iTRAQ Procedure and LC-MS Analysis

Total cell lysates were prepared from HD33i.8, HD60i.4, and 180i.5 cell lines (two duplicate samples from each cell line), and the proteins were precipitated with TCA and subjected to the iTRAQ procedure.

HPLC Analysis of Adenine Nucleotides

HPLC analysis was performed on NPCs to analyze quantitative differences on cellular ATP/ADP ratios, as described in the Supplemental Experimental Procedures.

Phalloidin Assay

For phalloidin staining, cells were incubated in phalloidin reagent, as described in the Supplemental Experimental Procedures.

Cell Cluster Formation Assay

Dissociated NPCs were plated and clump size was measured after 12 hr, as described in the Supplemental Experimental Procedures.

ACCESSION NUMBERS

All the information on microarray, including the raw data, is available online at the GEO webiste (accession code GSE37517).

SUPPLEMENTAL INFORMATION

Supplemental Information for this article includes six tables, six figures, Supplemental Experimental Procedures, and a list of consortium members and can be found with this article online at http://dx.doi.org/10.1016/j.stem.2012.04.027.

ACKNOWLEDGMENTS

We thank HD patients and their families for their essential contributions to this research and Nissim Benvenisty for critical reading. Primary support for this work was from RC2-NS069422 (L.M.T., C.N.S., J.F.G., C.A.R., and S.F.) and from the CHDI Foundation, Inc. (E.C., N.A., and P.K.). Additional support was provided by P50NS16375, P50NS16367 (HD Center Without Walls), and R01NS32765; CIRM fellowships TG2-01160 (J.A.K.) and TG2-01152 (A.K.); CIRM New Cell Line Grant RL1-00678-1 (L.M.T.); the Taube-Koret Center and the Hellman Family Foundation (S.F.); the Charlotte Geyer Foundation (J.T.); and NIH grant PO1 GM081629 (J.T.). Full membership of the HD iPSC Consortium is provided in Document S2.

Received: September 15, 2011
Revised: February 2, 2012
Accepted: April 19, 2012
Published online: June 28, 2012

REFERENCES

Apostol, B.L., Simmons, D.A., Zuccato, C., Illes, K., Pallos, J., Casale, M., Conforti, P., Ramos, C., Roarke, M., Kathuria, S., et al. (2008). CEP-1347 reduces mutant huntingtin-associated neurotoxicity and restores BDNF levels in R6/2 mice. Mol. Cell. Neurosci. *39*, 8–20.

Arrasate, M., and Finkbeiner, S. (2005). Automated microscope system for determining factors that predict neuronal fate. Proc. Natl. Acad. Sci. USA *102*, 3840–3845.

Arrasate, M., Mitra, S., Schweitzer, E.S., Segal, M.R., and Finkbeiner, S. (2004). Inclusion body formation reduces levels of mutant huntingtin and the risk of neuronal death. Nature *431*, 805–810.

Aubry, L., Bugi, A., Lefort, N., Rousseau, F., Peschanski, M., and Perrier, A.L. (2008). Striatal progenitors derived from human ES cells mature into DARPP32 neurons in vitro and in quinolinic acid-lesioned rats. Proc. Natl. Acad. Sci. USA *105*, 16707–16712.

Bae, B.I., Xu, H., Igarashi, S., Fujimuro, M., Agrawal, N., Taya, Y., Hayward, S.D., Moran, T.H., Montell, C., Ross, C.A., et al. (2005). p53 mediates cellular dysfunction and behavioral abnormalities in Huntington's disease. Neuron *47*, 29–41.

Behrens, P.F., Franz, P., Woodman, B., Lindenberg, K.S., and Landwehrmeyer, G.B. (2002). Impaired glutamate transport and glutamate-glutamine cycling: downstream effects of the Huntington mutation. Brain *125*, 1908–1922.

Blain, J.F., Paradis, E., Gaudreault, S.B., Champagne, D., Richard, D., and Poirier, J. (2004). A role for lipoprotein lipase during synaptic remodeling in the adult mouse brain. Neurobiol. Dis. *15*, 510–519.

Bradley, C.K., Scott, H.A., Chami, O., Peura, T.T., Dumevska, B., Schmidt, U., and Stojanov, T. (2011). Derivation of Huntington's disease-affected human embryonic stem cell lines. Stem Cells Dev. *20*, 495–502.

Camnasio, S., Carri, A.D., Lombardo, A., Grad, I., Mariotti, C., Castucci, A., Rozell, B., Riso, P.L., Castiglioni, V., Zuccato, C., et al. (2012). The first reported generation of several induced pluripotent stem cell lines from homozygous and heterozygous Huntington's disease patients demonstrates mutation related enhanced lysosomal activity. Neurobiol. Dis. *46*, 41–51.

Consortium, T.H.; The Huntington's Disease Collaborative Research Group. (1993). A novel gene containing a trinucleotide repeat that is expanded and unstable on Huntington's disease chromosomes. Cell *72*, 971–983.

Ebert, A.D., Yu, J., Rose, F.F., Jr., Mattis, V.B., Lorson, C.L., Thomson, J.A., and Svendsen, C.N. (2009). Induced pluripotent stem cells from a spinal muscular atrophy patient. Nature *457*, 277–280.

Faideau, M., Kim, J., Cormier, K., Gilmore, R., Welch, M., Auregan, G., Dufour, N., Guillermier, M., Brouillet, E., Hantraye, P., et al. (2010). In vivo expression of polyglutamine-expanded huntingtin by mouse striatal astrocytes impairs glutamate transport: a correlation with Huntington's disease subjects. Hum. Mol. Genet. *19*, 3053–3067.

Fan, M.M., and Raymond, L.A. (2007). N-methyl-D-aspartate (NMDA) receptor function and excitotoxicity in Huntington's disease. Prog. Neurobiol. *81*, 272–293.

Ginés, S., Paoletti, P., and Alberch, J. (2010). Impaired TrkB-mediated ERK1/2 activation in huntington disease knock-in striatal cells involves reduced p52/p46 Shc expression. J. Biol. Chem. *285*, 21537–21548.

Hodges, A., Strand, A.D., Aragaki, A.K., Kuhn, A., Sengstag, T., Hughes, G., Elliston, L.A., Hartog, C., Goldstein, D.R., Thu, D., et al. (2006). Regional and cellular gene expression changes in human Huntington's disease brain. Hum. Mol. Genet. *15*, 965–977.

Jacobsen, J.C., Gregory, G.C., Woda, J.M., Thompson, M.N., Coser, K.R., Murthy, V., Kohane, I.S., Gusella, J.F., Seong, I.S., MacDonald, M.E., et al. (2011). HD CAG-correlated gene expression changes support a simple dominant gain of function. Hum. Mol. Genet. *20*, 2846–2860.

Karasinska, J.M., and Hayden, M.R. (2011). Cholesterol metabolism in Huntington disease. Nat. Rev. Neurol. *7*, 561–572.

Koch, P., Breuer, P., Peitz, M., Jungverdorben, J., Kesavan, J., Poppe, D., Doerr, J., Ladewig, J., Mertens, J., Tüting, T., et al. (2011). Excitation-induced ataxin-3 aggregation in neurons from patients with Machado-Joseph disease. Nature *480*, 543–546.

Langbehn, D.R., Hayden, M.R., and Paulsen, J.S.; PREDICT-HD Investigators of the Huntington Study Group. (2010). CAG-repeat length and the age of onset in Huntington disease (HD): a review and validation study of statistical approaches. Am. J. Med. Genet. B. Neuropsychiatr. Genet. *153B*, 397–408.

Lievens, J.C., Rival, T., Iche, M., Chneiweiss, H., and Birman, S. (2005). Expanded polyglutamine peptides disrupt EGF receptor signaling and glutamate transporter expression in Drosophila. Hum. Mol. Genet. *14*, 713–724.

Luthi-Carter, R., Strand, A., Peters, N.L., Solano, S.M., Hollingsworth, Z.R., Menon, A.S., Frey, A.S., Spektor, B.S., Penney, E.B., Schilling, G., et al. (2000). Decreased expression of striatal signaling genes in a mouse model of Huntington's disease. Hum. Mol. Genet. *9*, 1259–1271.

Mattis, V.B., and Svendsen, C.N. (2011). Induced pluripotent stem cells: a new revolution for clinical neurology? Lancet Neurol. *10*, 383–394.

Miller, J.P., Holcomb, J., Al-Ramahi, I., de Haro, M., Gafni, J., Zhang, N., Kim, E., Sanhueza, M., Torcassi, C., Kwak, S., et al. (2010). Matrix metalloproteinases are modifiers of huntingtin proteolysis and toxicity in Huntington's disease. Neuron *67*, 199–212.

Molero, A.E., Gokhan, S., Gonzalez, S., Feig, J.L., Alexandre, L.C., and Mehler, M.F. (2009). Impairment of developmental stem cell-mediated striatal neurogenesis and pluripotency genes in a knock-in model of Huntington's disease. Proc. Natl. Acad. Sci. USA *106*, 21900–21905.

Nguyen, H.N., Byers, B., Cord, B., Shcheglovitov, A., Byrne, J., Gujar, P., Kee, K., Schüle, B., Dolmetsch, R.E., Langston, W., et al. (2011). LRRK2 mutant iPSC-derived DA neurons demonstrate increased susceptibility to oxidative stress. Cell Stem Cell *8*, 267–280.

Park, I.H., Arora, N., Huo, H., Maherali, N., Ahfeldt, T., Shimamura, A., Lensch, M.W., Cowan, C., Hochedlinger, K., and Daley, G.Q. (2008). Disease-specific induced pluripotent stem cells. Cell *134*, 877–886.

Pruunsild, P., Sepp, M., Orav, E., Koppel, I., and Timmusk, T. (2011). Identification of cis-elements and transcription factors regulating neuronal activity-dependent transcription of human BDNF gene. J. Neurosci. *31*, 3295–3308.

Reis, S.A., Thompson, M.N., Lee, J.M., Fossale, E., Kim, H.H., Liao, J.K., Moskowitz, M.A., Shaw, S.Y., Dong, L., Haggarty, S.J., et al. (2011). Striatal neurons expressing full-length mutant huntingtin exhibit decreased N-cadherin and altered neuritogenesis. Hum. Mol. Genet. *20*, 2344–2355.

Rosenblatt, A., Kumar, B.V., Mo, A., Welsh, C.S., Margolis, R.L., and Ross, C.A. (2012). Age, CAG repeat length, and clinical progression in Huntington's disease. Mov. Disord. *27*, 272–276.

Ross, C.A., and Poirier, M.A. (2004). Protein aggregation and neurodegenerative disease. Nat. Med. Suppl. *10*, S10–S17.

Ross, C.A., and Tabrizi, S.J. (2011). Huntington's disease: from molecular pathogenesis to clinical treatment. Lancet Neurol. *10*, 83–98.

Ross, C.A., and Thompson, L.M. (2006). Transcription meets metabolism in neurodegeneration. Nat. Med. *12*, 1239–1241.

Royer, B., Soares, D.C., Barlow, P.N., Bontrop, R.E., Roll, P., Robaglia-Schlupp, A., Blancher, A., Levasseur, A., Cau, P., Pontarotti, P., and Szepetowski, P. (2007). Molecular evolution of the human SRPX2 gene that causes brain disorders of the Rolandic and Sylvian speech areas. BMC Genet. *8*, 72.

Seibler, P., Graziotto, J., Jeong, H., Simunovic, F., Klein, C., and Krainc, D. (2011). Mitochondrial Parkin recruitment is impaired in neurons derived from mutant PINK1 induced pluripotent stem cells. J. Neurosci. *31*, 5970–5976.

Seong, I.S., Ivanova, E., Lee, J.M., Choo, Y.S., Fossale, E., Anderson, M., Gusella, J.F., Laramie, J.M., Myers, R.H., Lesort, M., and MacDonald, M.E. (2005). HD CAG repeat implicates a dominant property of huntingtin in mitochondrial energy metabolism. Hum. Mol. Genet. *14*, 2871–2880.

Shelbourne, P.F., Keller-McGandy, C., Bi, W.L., Yoon, S.R., Dubeau, L., Veitch, N.J., Vonsattel, J.P., Wexler, N.S., Arnheim, N., and Augood, S.J.; US-Venezuela Collaborative Research Group. (2007). Triplet repeat mutation length gains correlate with cell-type specific vulnerability in Huntington disease brain. Hum. Mol. Genet. *16*, 1133–1142.

Stine, O.C., Pleasant, N., Franz, M.L., Abbott, M.H., Folstein, S.E., and Ross, C.A. (1993). Correlation between the onset age of Huntington's disease and length of the trinucleotide repeat in IT-15. Hum. Mol. Genet. *2*, 1547–1549.

Svendsen, C.N., ter Borg, M.G., Armstrong, R.J., Rosser, A.E., Chandran, S., Ostenfeld, T., and Caldwell, M.A. (1998). A new method for the rapid and long term growth of human neural precursor cells. J. Neurosci. Methods *85*, 141–152.

Takahashi, K., Tanabe, K., Ohnuki, M., Narita, M., Ichisaka, T., Tomoda, K., and Yamanaka, S. (2007). Induction of pluripotent stem cells from adult human fibroblasts by defined factors. Cell *131*, 861–872.

Takata, K., Kitamura, Y., Tsuchiya, D., Kawasaki, T., Taniguchi, T., and Shimohama, S. (2004). High mobility group box protein-1 inhibits microglial Abeta clearance and enhances Abeta neurotoxicity. J. Neurosci. Res. *78*, 880–891.

Túnez, I., Sánchez-López, F., Agüera, E., Fernández-Bolaños, R., Sánchez, F.M., and Tasset-Cuevas, I. (2011). Important role of oxidative stress biomarkers in Huntington's disease. J. Med. Chem. *54*, 5602–5606.

Vonsattel, J.P., Keller, C., and Del Pilar Amaya, M. (2008). Neuropathology of Huntington's disease. Handb. Clin. Neurol. *89*, 599–618.

Walker, F.O. (2007). Huntington's disease. Lancet *369*, 218–228.

Xu, E.H., Tang, Y., Li, D., and Jia, J.P. (2009). Polymorphism of HD and UCHL-1 genes in Huntington's disease. J. Clin. Neurosci. *16*, 1473–1477.

Yu, J., Vodyanik, M.A., Smuga-Otto, K., Antosiewicz-Bourget, J., Frane, J.L., Tian, S., Nie, J., Jonsdottir, G.A., Ruotti, V., Stewart, R., et al. (2007). Induced pluripotent stem cell lines derived from human somatic cells. Science *318*, 1917–1920.

Yu, J., Hu, K., Smuga-Otto, K., Tian, S., Stewart, R., Slukvin, I.I., and Thomson, J.A. (2009). Human induced pluripotent stem cells free of vector and transgene sequences. Science *324*, 797–801.

Zhang, N., An, M.C., Montoro, D., and Ellerby, L.M. (2010). Characterization of Human Huntington's Disease Cell Model from Induced Pluripotent Stem Cells. PLoS Curr *2*, RRN1193.

Zuccato, C., and Cattaneo, E. (2009). Brain-derived neurotrophic factor in neurodegenerative diseases. Nat. Rev. Neurol. *5*, 311–322.

Zuccato, C., Valenza, M., and Cattaneo, E. (2010). Molecular mechanisms and potential therapeutical targets in Huntington's disease. Physiol. Rev. *90*, 905–981.